Journal of Renewable Materials

Tech Science Press

https://doi.org/10.32604/jrm.2026.02026-0040

ARTICLE

Mussel Shell Waste as a Bio-Filler in PLLA: Effects on Crystallization, Thermal and Mechanical Performance

Nathan Jourdainne[1,2], Mathilda Ekholm[1], Nawel Belkessa[1], Antonin Vignon[1], Nicolas Sbirrazzuoli[1], Christelle Combeaud[2], Jean-Luc Bouvard[2] and Nathanael Guigo[1,2,*]

[1]Nice Institute of Chemistry (CNRS UMR 7272), University Côte d'Azur, Valrose Avenue, 28, Nice, France
[2]Mines Paris, PSL University, CEMEF (CNRS UMR 7635), Sophia Antipolis, France

*Corresponding Author: Nathanael Guigo. Email: nathanael.guigo@minesparis.psl.eu

Received: 18 March 2026; Accepted: 06 May 2026; Published: 28 July 2026

ABSTRACT: This study investigates the valorization of mussel shell waste as a bio-derived filler in poly(L-lactic acid) (PLLA) to promote sustainable materials aligned with circular economy principles. Mussel shells, a seafood industry byproduct rich in biogenic calcium carbonate, were ground into powder and incorporated into PLLA at 10–50 wt%. The resulting composites were thoroughly characterized using scanning electron microscopy and energy dispersive X-ray spectroscopy (SEM-EDX), Fourier transform infrared spectroscopy (FTIR), thermogravimetric analysis (TGA), differential scanning calorimetry (DSC), dynamic mechanical thermal analysis (DMTA), and uniaxial tensile testing to assess morphological, chemical, thermal, and mechanical properties. Incorporation of mussel shell powder significantly increased stiffness, with the storage modulus improving by more than 70% at the highest filler content. DSC results suggest that mussel shell powder promotes a heterogeneous nucleation effect in PLLA, enhancing crystallization and modifying crystallization behavior. DMTA measurements further demonstrated a substantial increase in thermomechanical stiffness while only slightly affecting the glass transition temperature, indicating restricted chain mobility due to the presence of the rigid mineral filler. TGA revealed a second degradation step from calcium carbonate decomposition, without compromising processability. Conversely, tensile strength, ductility, and toughness decreased progressively, reflecting the typical stiffness-toughness trade-off of mineral-filled composites. Overall, this work highlights the potential of mussel shell powder not only as a sustainable bio-derived filler but also as a functional reinforcing phase that can influence crystallization behavior and thermomechanical performance of PLLA.

KEYWORDS: Biogenic; biodegradable polymers; composite materials; mechanical properties; thermal properties; scanning electron microscopy

1 Introduction

As the global population and industrial activity grow [1], there is an increasing demand for chemicals and materials [2], but as most polymers and chemicals are derived from fossil fuel resources [3], this poses significant environmental risks [4]. Around the world, the production and use of materials are increasingly constrained by environmental limits, affecting everything from biodiversity and land use to climate systems and nutrient cycles [5]. Addressing the environmental footprint of material consumption is both urgent and complex, demanding progressive evaluation of potential side effects and the integration of multidisciplinary systems-based strategies [5].

Polylactic acid (PLA), and in particular its L-isomer-rich form poly(L-lactic acid) (PLLA), is a biodegradable thermoplastic derived from biomass such as corn or sugarcane [6]. Owing to its compostability [7], biocompatibility [8], and mechanical performance [9], PLLA has gained prominence as an eco-friendly alternative to conventional plastics [10]. However, its cost, thermal resistance, and mechanical brittleness often limit broader application [6,11,12]. One widely studied approach to address these limitations involves incorporating solid fillers into PLLA to tailor its performance and reduce reliance on virgin polymer [12,13].

Previous studies have shown that the incorporation of fillers into polymer matrices can significantly enhance stiffness and thermal stability [14]. For instance, mineral or bio-based fillers in PLA and epoxy systems have been reported to increase Young's modulus by 20%–100%, depending on filler type, loading, and dispersion, although often at the expense of ductility and toughness [15,16]. Such improvements highlight the potential of filler incorporation as an effective strategy to tailor polymer performance.

While traditional mineral fillers (e.g., talc, glass, calcium carbonate) are effective, they are non-renewable and often associated with high environmental extraction costs [17]. Recent studies have explored bio-based fillers, such as wood flour [18], cotton [19], and agricultural byproducts [20,21], for their potential to reduce environmental impact while maintaining or enhancing composite properties [13]. In particular, fillers derived from waste streams offer a dual advantage: performance enhancement and waste valorization [11].

In addition to stiffness enhancement, the fracture behavior of filled polymers is a key parameter in structural applications. Fracture energy and toughness are intrinsic properties governing crack initiation and propagation, particularly relevant for finite element analysis (FEA) and engineering design [22,23]. However, incorporation of rigid fillers often leads to reduced fracture energy due to stress concentration and limited plastic deformation [24], emphasizing the need to balance stiffness and toughness in composite design.

More recently, renewable fillers have also been incorporated into biodegradable polymer blends to tailor both environmental and material performance. For example, Letwaba et al. [25] investigated PLA/PBAT blends reinforced with algae biomass and studied their biodegradation behavior under controlled composting conditions. Their work showed that the incorporation of algae could accelerate biodegradation while influencing the thermal and morphological properties of the composites. Such studies highlight the growing interest in bio-derived fillers for improving the sustainability of biodegradable polymers. However, most of these investigations focus primarily on biodegradation performance and organic biomass fillers, while comparatively fewer studies have examined the potential of biogenic mineral fillers derived from biological waste to modify the crystallization behavior and thermomechanical properties of PLA-based materials.

Recent research has shown that incorporating bio-based fillers into polylactic acid composites can significantly reduce environmental impacts compared to conventional inorganic fillers [17]. In a combined life cycle and techno-economic assessment, fillers such as wood, flax, and dried distillers' grains with solubles (DDGS) demonstrated lower greenhouse gas emissions, reduced energy consumption, and lower production costs than traditional fillers like glass and talc [26]. As a result, bio-based fillers represent a promising route to enhance the sustainability of PLA composites without compromising performance, supporting the broader shift toward greener material solutions [17].

From a life-cycle perspective, the use of waste-derived fillers such as shellfish byproducts offers additional environmental benefits by reducing landfill disposal, lowering raw material extraction, and contributing to circular economy strategies [27]. Compared to conventional mineral fillers obtained through mining, biogenic calcium carbonate can significantly reduce environmental footprint while enabling resource recovery from food industry waste streams.

As the global population grows, food waste is also rising, with production and disposal increasing in parallel [28]. When left to decompose or incinerated, this waste contributes to additional environmental harm. While traditionally extracted from limestone quarries, substitutes derived from biological sources like eggshells or seashells are more interesting from an environmental perspective, as they can lower resource depletion and valorize products that would otherwise be considered food waste [29].

Among potential bio-waste fillers, shellfish waste such as mussel shells presents an untapped opportunity. Composed predominantly of biogenic calcium carbonate (i.e., aragonite or calcite) [30], mussel shells are an abundant byproduct of the seafood industry yet are commonly discarded in landfills or incinerated [31]. Compared to mined $CaCO_3$, biogenic sources may reduce resource depletion and associated emissions, while providing a route for upcycling food waste into high-value materials [32].

Mussel shells exhibit a hierarchical structure composed of calcium carbonate crystals (typically aragonite) embedded in an organic matrix, providing intrinsic mechanical robustness [30]. This unique structure, combined with trace elements such as Mg and Sr, may influence interfacial interactions with polymer matrices and potentially affect crystallization behavior [33]. Furthermore, biogenic $CaCO_3$ has been increasingly investigated as a sustainable alternative filler in polymer composites, where it can act as a reinforcing phase and influence thermal and mechanical properties [34].

Although biogenic calcium carbonate from eggshells or clams has been used in polymer matrices, the use of mussel shells in PLA-based composites remains largely underexplored. Given their unique morphology, trace mineral composition (e.g., Mg, Sr), and marine origin, mussel shells may offer distinctive advantages as reinforcing fillers.

In particular, biogenic $CaCO_3$ fillers have been reported to influence the crystallization behavior of PLLA by providing heterogeneous nucleation sites, which can modify crystallization kinetics and final microstructure [35]. However, the extent of this effect depends strongly on filler characteristics such as particle size, dispersion, and interfacial interactions [36].

The aim of this study is to investigate the incorporation of mussel shell powder into PLLA to assess its impact on thermal and mechanical properties. A comprehensive characterization—using techniques such as SEM-EDX, FTIR, TGA, DSC, DMA, and tensile testing—is carried out to understand filler-matrix interactions and the overall composite performance. This work proposes a new valorization pathway for shellfish waste while advancing the development of functional, sustainable bio-composites.

The novelty of this work lies in the combined investigation of thermomechanical behavior and crystallization phenomena in PLLA filled with mussel shell-derived biogenic calcium carbonate over a wide filler loading range (10–50 wt%), with a particular focus on linking filler characteristics to structure-property relationships. In addition, this study contributes to the development of sustainable materials by demonstrating a viable route for converting marine bio-waste into value-added polymer composites. Potential applications of such materials include packaging, semi-structural components, and biodegradable products where enhanced stiffness and reduced environmental impact are desired.

2 Experimental

2.1 Materials

Mytillus galloprovincialis mussels were collected near the coast of Saint-Jean-Cap-Ferrat (43°41′ 02.4″ N, 7°18′56.2″ E), France, by the "Moyens à la Mer" technical service of the Laboratoire Océanographique de Villefranche-sur-Mer (FR3761, Mediterranean Sea). After collection, the mussels were manually dissected, and the shells were separated from the soft tissues.

Poly(L-lactic acid) (PLLA) was provided by Total Corbion under the trade name Luminy® LX175. According to the supplier, LX175 is a high-viscosity grade suitable for film extrusion and thermoforming. All polymers were used as received, without any further purification or chemical modification.

2.2 Material Fabrication

Mussel shells were first opened, cleaned, and dried overnight in a vacuum oven at 80°C to remove moisture and any remaining organic residues. The dried shells were then processed into a fine powder using a cryogenic ball mill (GT-300, Powtec). To prevent heating during the grinding process, liquid nitrogen was added prior to milling. Grinding was performed for 5 min at 1000 rpm.

Composite films were prepared by mixing poly(L-lactic acid) (PLLA) with mussel shell powder at different weight ratios: 0%, 10%, 20%, 30%, 40%, and 50% *w/w*. Neat PLLA (0 wt%) was processed following the same thermal and pressing protocol as the composite samples, but without the addition of mussel shell powder. PLLA was first melted at 260°C directly in a PDMS mold. Once fully molten, the corresponding amount of mussel shell powder was added and manually mixed into the polymer melt to ensure uniform dispersion.

The resulting molten mixture was then placed between two flat Kapton® sheets and transferred to a hot press. The system was compressed quickly at 190°C under a pressure of approximately 10–15 bar to form a film. After pressing, the sample was removed from the press and allowed to cool naturally on a flat surface at room temperature to solidify. The final films had a thickness of approximately 300–400 μm, suitable for subsequent characterization.

It should be noted that the processing temperature of 260°C was selected to ensure complete melting and adequate flow of PLLA, particularly at high filler loadings where viscosity increases significantly. To limit potential thermal degradation, the residence time at this temperature was kept as short as possible. The subsequent hot-pressing step at 190°C was performed below the typical degradation onset of PLLA, thereby minimizing additional thermal damage.

2.3 Testing Procedures

2.3.1 Scanning Electron Microscopy and Energy Dispersive X-Ray Spectroscopy (SEM-EDX)

Mussel shell powder was deposited on carbon double tape, fixed on a copper sample holder. Deposit was carbon-coated and SEM-EDX were performed using a Tescan Vega3 XMU Scanning Electron Microscope (Tescan France, Fuveau, France) equipped with an Oxford X-MaxN 50 mm^2 EDX detector (Oxford Instruments, Abingdon, UK). SEM images were obtained in secondary electron mode, at 20 kV.

2.3.2 Fourier Transform Infrared Spectroscopy (FTIR)

Sample was analyzed by FTIR spectroscopy. The spectra were acquired between 4000 and 400 cm^{-1} with a Bruker TENSOR 27 spectrophotometer employed in attenuated total reflectance (ATR) mode using a diamond crystal. 32 scans were accumulated with a resolution of 4 cm^{-1}.

2.3.3 Thermogravimetric Analysis (TGA)

TGA measurements were carried out using a TGA 2 instrument from Mettler-Toledo. Samples were placed in 70 μL alumina crucibles and heated from 25°C to 900°C at a constant heating rate of 5°C/min under a nitrogen flow of 50 mL/min. The data were processed and analyzed using the STARe 18.00 thermal analysis software.

2.3.4 Differential Scanning Calorimetry (DSC)

DSC measurements were performed using a DSC 822 instrument (Mettler Toledo), equipped with a Huber IntraCooler TC45. The DSC system utilizes a highly sensitive HSS7 ceramic sensor (heat-flux sensor with 120 Au–Au/Pd thermocouples), ensuring precise thermal measurements. To maintain accuracy, temperature, enthalpy, and tau lag calibrations were routinely conducted using indium and zinc standards. Approximately 4.5–5.5 mg of sample material was sealed in 40 µL pierced aluminum pans. Measurements were carried out from 5°C to 210°C at a heating rate of 10°C/min, under an air atmosphere with a constant flow rate of 50 mL/min. The T_g was identified as the inflection point of the baseline deviation in the reversing heat flow signal. The data were processed and analyzed using the STARe 18.00 thermal analysis software.

The crystallization conversion, $\alpha(T)$, was calculated from the partial area of the exotherm as a function of temperature according to:

$$\alpha(T) = \frac{\int_{T_0}^{T} q(T)\,dT}{\int_{T_0}^{T_f} q(T)\,dT} \tag{1}$$

with $q(T)$ is the heat flow associated with crystallization, and T_0 and T_f correspond to the onset and end temperatures of the crystallization event, respectively. Conversion curves were reported as $\alpha(T)$ vs. temperature.

Because only PLLA contributes to crystallization, the crystallization enthalpy was also normalized to the PLLA mass fraction in the composites. The PLLA fraction, w_{PLLA}, was determined from the filler content estimated by TGA, and the crystallization enthalpy of PLLA was calculated as:

$$\Delta Hc_{PLLA} = \frac{\Delta Hc_{sample}}{w_{PLLA}} \tag{2}$$

with

$$w_{PLLA} = 1 - w_{filler} \tag{3}$$

To investigate crystallization upon heating, samples were first erased of their thermal history by melting at 220°C for 10 min in a convection oven. Immediately after melting, the aluminum pans were rapidly quenched by immersion in liquid nitrogen to obtain an amorphous state. The quenched samples were then subjected to a DSC heating scan from 5°C to 210°C at a rate of 10°C/min under the same experimental conditions described above.

The degree of crystallinity (χ_c) for each sample was determined according to Eq. (4):

$$\chi_c = \frac{\Delta H_m - \Delta H_c}{\Delta H_m^0} \times 100 \tag{4}$$

where ΔH_m (J g^{-1}) is the melting enthalpy calculated from the endothermic peak integration obtained from the first heating scan; ΔH_c (J g^{-1}) is the sample crystallization enthalpy calculated from the exothermic peak integration obtained from the first heating scan; ΔH_m^0 is the theoretical melting enthalpy of the polymer assumed to be 100% crystalline: 93 J g^{-1} for PLLA [37].

2.3.5 Dynamic Mechanical Analysis (DMA)

Dynamic mechanical analysis (DMA) was performed using a DMA 1 analyzer from Mettler-Toledo in tensile mode to evaluate the thermomechanical behavior of the PLLA/mussel shell powder composite

films. Rectangular specimens with dimensions of 5 × 3 × 0.35 mm (length × width × thickness) were tested. The temperature sweep was conducted from 10°C to 230°C at a constant heating rate of 2°C/min. A single-frequency oscillation mode was used, with a frequency of 1 Hz, a displacement amplitude of 5 μm, and a strain amplitude of 0.1% under auto-tension offset control. The storage modulus (E'), loss modulus (E''), and damping factor (tan δ) were recorded as functions of temperature. The data were analyzed using the STARe 18.00 thermal analysis software.

2.3.6 Uniaxial Tensile Testing

Tensile measurements were performed in a Shimadzu testing machine using a crosshead speed of 1 mm/min, with a load cell of 1 kN. All specimens were cut in dumbbell shape, i.e., 21 × 2.0 × 0.4 mm (length × width × thickness). A minimum of 6 measurements was carried out for each sample, and the results were used to calculate the mean values of Young's Modulus, maximum stress, stress at rupture, toughness and elongation at break.

3 Results and Discussion

3.1 Morphological and Particle Size Characterization (SEM)

Scanning electron microscopy (SEM) was conducted on the mussel shell powder. Obtained images are shown in Fig. 1.

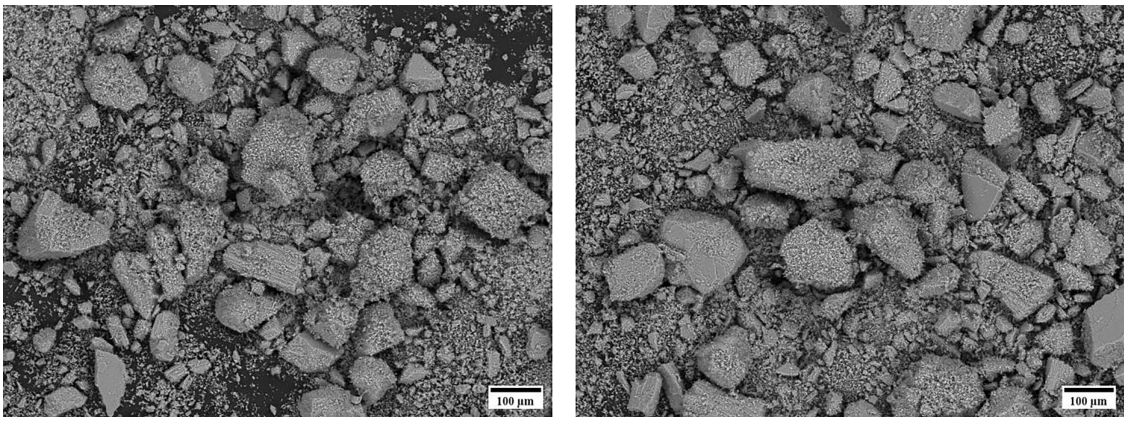

Figure 1: SEM images of mussel shell powder.

Scanning electron microscopy coupled with energy dispersive X-ray spectroscopy (SEM-EDX) was performed to characterize the morphology, particle size distribution, and elemental composition of the mussel shell powder, which are expected to influence filler dispersion within the PLLA matrix as well as its potential nucleating and reinforcing effects. SEM images revealed that the mussel shell powder exhibited a heterogeneous distribution of particle sizes and shapes, including angular, flaky, and irregular geometries. Particle sizes vary between few micrometers up to 200 μm. This morphological heterogeneity is typical of ground biogenic materials [38] and can be attributed to the mechanical grinding process, which fractures the shell into particles along natural cleavage planes or microstructural weak points. Such diversity in particle morphology and size distribution can significantly influence the filler-polymer interactions.

Irregular shapes may lead to mechanical interlocking within the polymer matrix, enhancing stiffness [39]. Wide size distribution can promote better packing within the polymer but may also lead to

inconsistent dispersion or agglomeration, potentially contributing to localized stress concentrations or defects [40].

3.2 Elemental Composition (EDX)

Energy Dispersive X-ray (EDX) spectra were collected on mussel shell powder spots, and average spectra were also collected through elemental maps (not shown). Since similar observations were made in different analyzed spots and areas, one averaged spectrum is shown in Fig. 2.

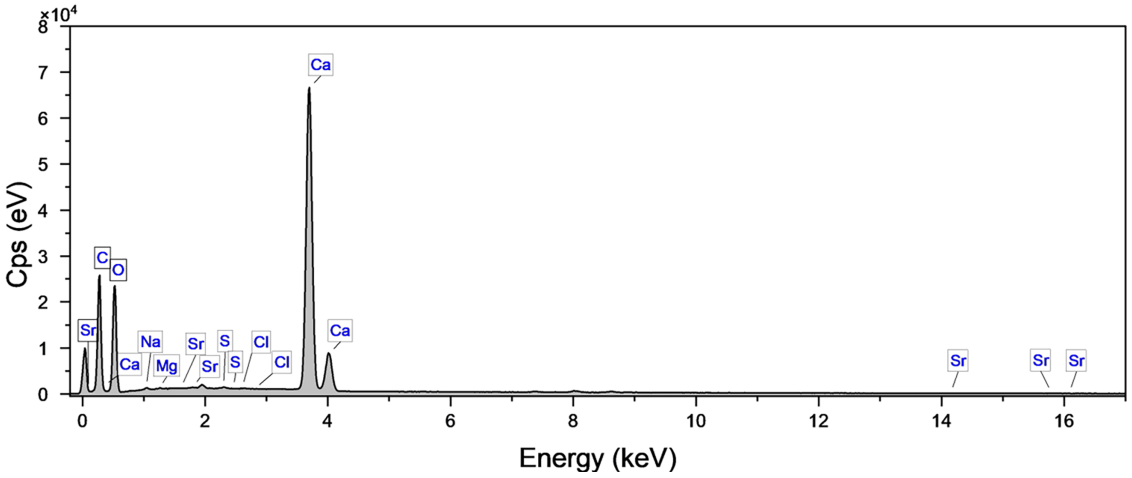

Figure 2: EDX spectrum of mussel shell powder.

EDX results showed calcium (Ca) as major element in the mussel shell powder, associated with calcium carbonate ($CaCO_3$), confirming that the primary inorganic constituent is aragonite and calcite, consistent with known shell composition [41]. Trace elements such as Sodium (Na), Magnesium (Mg), and Strontium (Sr) were also detected in smaller amounts.

Strontium likely originates from seawater and is naturally incorporated into the calcium carbonate structure of marine shells. Its persistence after washing suggests it is structurally integrated rather than simply adsorbed at the surface. Magnesium is often considered as substitutes for calcium in biogenic carbonates, especially in aragonite phases, which are common in mollusk shells [42]. Its presence supports a natural compositional variability of the shell material, with Mg acting as a stabilizer of the crystalline form [43]. The presence of these minor elements could influence the interfacial chemistry with PLLA. These elements may also influence surface energy and wettability, thus affecting the dispersion and interfacial bonding between filler and polymer.

3.3 Chemical Structure Characterization (FTIR)

FTIR spectroscopy was conducted to investigate the chemical structure of mussel shell powder, neat PLLA, and PLLA-based composites containing 10% to 50% *w/w* mussel powder. The spectra confirm the presence of characteristic bands of both PLLA and mussel shell constituents as shown in Fig. 3.

The mussel shell powder (MP) spectrum displays prominent absorption bands at approximately 1410, 870, and 710 cm^{-1}, which are typical of calcium carbonate ($CaCO_3$) [44], particularly the in-plane bending (ν_4), out-of-plane bending (ν_2), and lattice mode vibrations, respectively. These bands are consistently observed in the composite films, confirming the presence and successful incorporation of mussel shell powder into the polymer matrix without chemical transformation. However, no systematic or proportional

increase in band intensity with increasing filler content is observed. This behavior is attributed to the use of ATR-FTIR, for which band intensities are not reliably proportional to filler concentration due to variations in contact pressure between sample and the diamond crystal and wavelength-dependant depth.

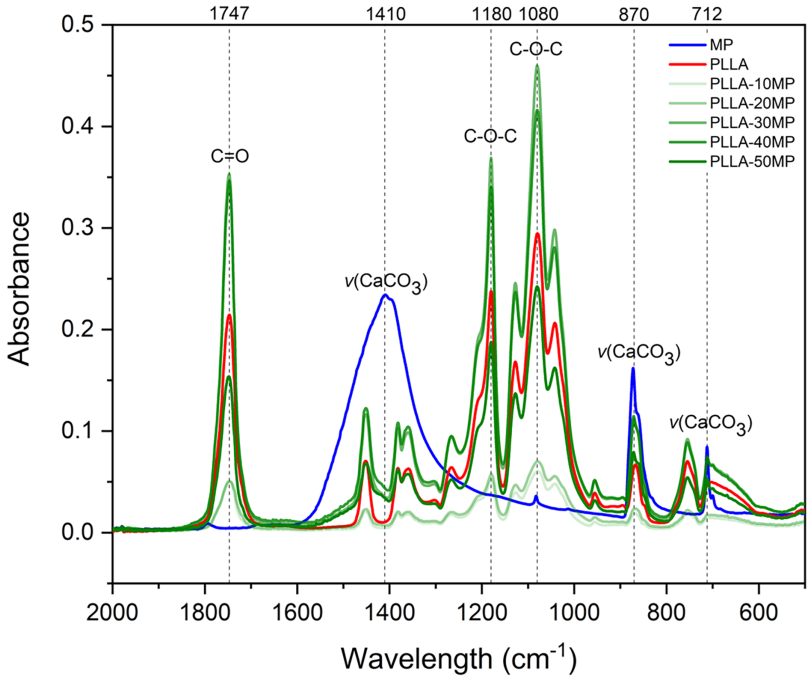

Figure 3: FTIR spectra of neat PLLA, mussel shell powder (MP), and PLLA-based composites containing 10%–50% *w/w* mussel shell powder.

Neat PLLA exhibits typical absorption bands at 1750 cm^{-1} (C=O stretching of the ester group) [45] and 1180–1080 cm^{-1} (C–O–C stretching) [46]. These bands remain unchanged across all composite spectra, indicating that no new chemical bonds or interactions were formed between the PLLA and the mussel powder during processing. Instead, the spectra suggest a physical mixing of the filler within the polymer matrix, with no evidence of chemical degradation or reaction.

Although $CaCO_3$-related bands are clearly detected in all composite samples, their relative intensity variations do not strictly follow the nominal filler content, which is consistent with the intrinsic limitations of ATR-FTIR for quantitative analysis of heterogeneous composites. Consequently, FTIR is used here as a qualitative tool to identify the chemical constituents of the composites, while quantitative assessment of mineral content is more reliably provided by thermogravimetric analysis.

3.4 Thermal Stability Assessment

Thermogravimetric analysis was conducted on neat PLLA and PLLA-mussel shell powder composite films with mussel powder mass fractions ranging from 10% to 50%, to assess their thermal stability and decomposition behavior under a nitrogen flow (Fig. 4).

Neat PLLA exhibited a single-step thermal degradation, with the onset of 1% mass loss occurring at 298.5°C (Table 1). As the mussel shell powder content increased, a progressive shift of the degradation onset toward lower temperatures was observed. For instance, the temperature corresponding to 1% mass loss decreased to 276.5°C for the 10 wt% composite and further to 255.8°C for the 50 wt% composite. A similar trend was observed for the temperatures at 5% and 10% mass loss, indicating a gradual reduction in the

thermal stability of the PLLA matrix upon filler incorporation. These results suggest that the presence of mussel shell powder slightly accelerates the initial degradation of PLLA.

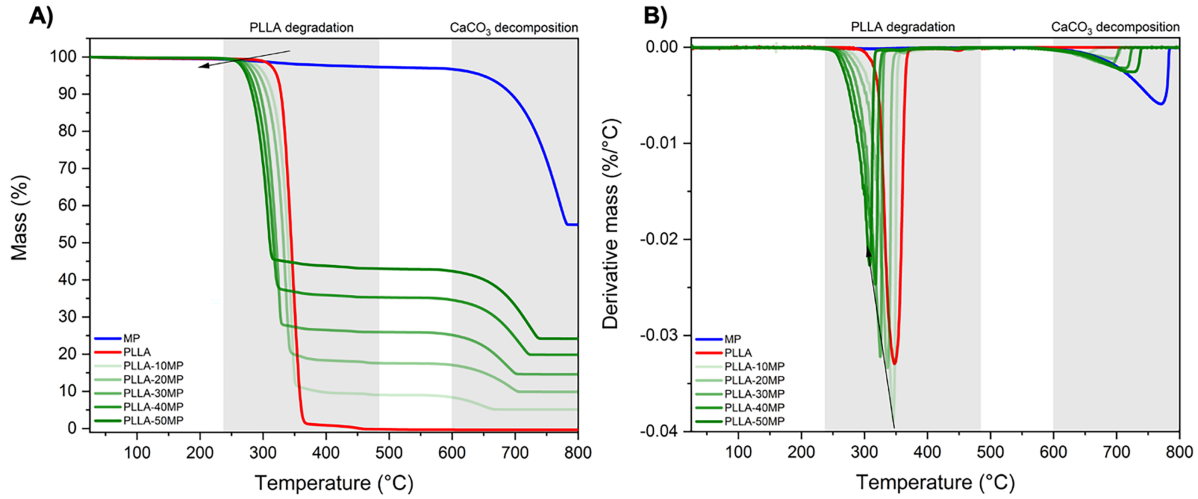

Figure 4: (**A**) TG and (**B**) dTG curves of PLLA, mussel shell powder, and PLLA/mussel shell powder composites (10%–50% *w/w*) measured at 10°C/min under nitrogen flow.

Table 1: Degradation onset temperatures at 1%, 5%, and 10% mass loss (T_{deg}) determined by TGA for PLLA/mussel shell powder composites.

PLLA/Mussel Shell Powder Ratio *(w/w)*	Mussel Shell Powder Ratio Estimated from TGA (%)	T_{deg} 1% (°C)	T_{deg} 5% (°C)	T_{deg} 10% (°C)
100/0	–	298.5	322.1	328.5
90/10	11.2	276.5	303.5	314.5
80/20	19.5	268.1	294.4	305.6
70/30	27.3	262.7	286.2	295.8
60/40	36.9	256.1	278.9	288.5
50/50	44.7	255.8	274.1	283.0
0/100	–	280.1	648.9	694.0

In addition to changes in degradation onset, the composite samples exhibited a second mass loss event at higher temperatures (above ~650°C), which was absent in neat PLLA. This second degradation step is attributed to the thermal decomposition of calcium carbonate ($CaCO_3$) from the mussel shell powder into calcium oxide (CaO) and carbon dioxide (CO_2) [47], in agreement with the TGA behavior of the pure mussel shell powder, which showed a major decarbonation step with a mass loss of approximately 42%.

The residual mass at high temperature increased systematically with increasing filler content, reflecting the presence of thermally stable inorganic material. Based on the residual mass after polymer degradation and the known decarbonation behavior of $CaCO_3$, the effective mussel shell powder content in the composites was estimated from the TGA data and is reported in Table 1. The estimated filler contents are in good agreement with the nominal formulations, yielding values of 11.2%, 19.5%, 27.3%, 36.9%, and 44.7% for the composites prepared with nominal loadings of 10, 20, 30, 40, and 50 wt%, respectively. This

confirms the successful and reproducible incorporation of the mussel shell powder into the PLLA matrix during processing.

The incorporation of mussel shell powder leads to a moderate decrease in the thermal stability of PLLA, which may be attributed to several combined effects, including disruption of polymer chain packing by the inorganic filler [48], possible catalytic effects induced by mineral surfaces [49], and the presence of trace elements such as magnesium and strontium in the biogenic calcium carbonate. These effects are consistent with previously reported behaviors of mineral-filled biodegradable polymer composites and remain limited in magnitude [50,51], indicating that the composites retain sufficient thermal stability for conventional melt-processing applications.

3.5 Thermal Transitions and Crystallization Behavior (DSC)

Differential scanning calorimetry (DSC) was performed to investigate the crystallization behavior of neat PLLA and PLLA/mussel shell powder composites under two different conditions: crystallization during cooling from the melt and crystallization upon heating after rapid quenching. This analysis allows evaluation of the influence of the biogenic calcium carbonate filler on nucleation processes, crystallization kinetics, and the overall semicrystalline structure of PLLA. DSC cooling thermograms and the corresponding crystallization conversion curves are shown in Fig. 5. The main thermal parameters extracted from these experiments are summarized in Tables 2 and 3.

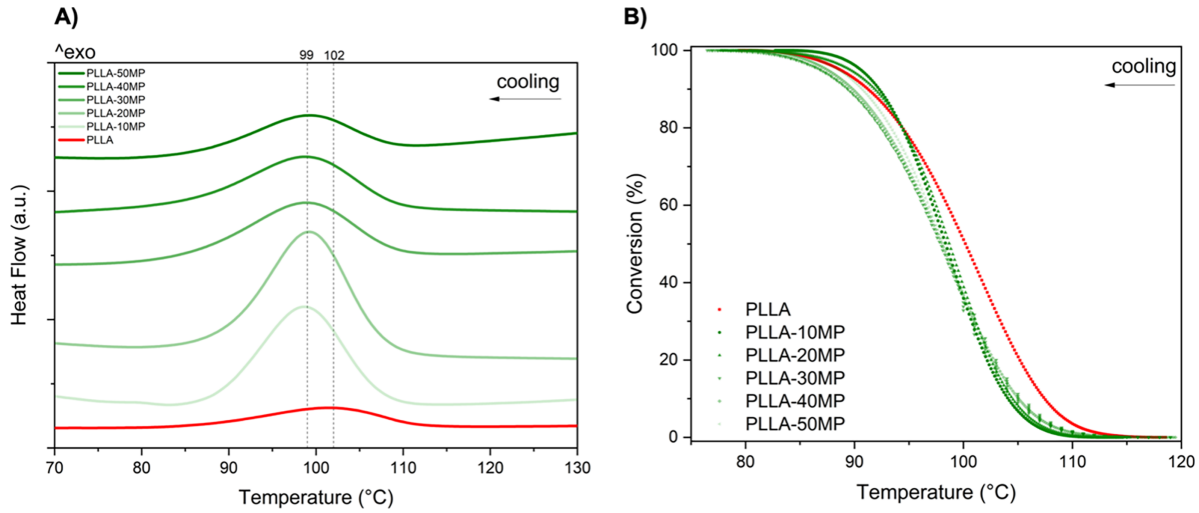

Figure 5: (**A**) Cooling scans and (**B**) conversion rate of PLLA and PLLA/mussel shell powder composites (10%–50% *w/w*) recorded by DSC at 10°C/min.

Table 2: Crystallization temperature (*Tc*) and enthalpy of crystallization (Δ*Hc*) of PLLA/mussel shell powder composites from DSC cooling scans at 10°C/min.

PLLA/Mussel Ratio	100/0	90/10	80/20	70/30	60/40	50/50
Tc (°C)	102.1	98.7	99.4	98.7	98.9	99.2
ΔHc (J/g sample)	7.1	26.5	33.2	19.3	17.7	10.9
PLLA fraction	1.000	0.888	0.805	0.727	0.631	0.553
ΔHc (J/g PLLA)	7.1	29.8	41.2	26.5	28.1	19.7

Table 3: Glass transition, crystallization, and melting parameters of neat PLLA and PLLA/mussel shell powder composites obtained by DSC heating scans at 10°C/min.

PLLA/Mussel Ratio	100/0	90/10	80/20	70/30	60/40	50/50
T_g (°C)	58.0	57.4	57.2	57.1	57.5	57.1
ΔCp (J/g/K)	0.686	0.772	0.692	0.642	0.469	0.375
Tc (°C)	106.8	103.5	102.9	104.7	103.8	103.6
ΔHc (J/g sample)	52.4	50.9	41.8	39.1	35.3	29.8
PLLA fraction	1.000	0.888	0.805	0.727	0.631	0.553
ΔHc (J/g PLLA)	52.4	57.3	51.9	53.8	55.9	53.9
Tm (°C)	168.7	169.0	168.3	168.1	167.1	166.2
ΔHm (J/g)	52.2	52.4	45.6	41.1	35.9	29.2
χ_c (%)	0	2	4	2	1	0

During cooling, neat PLLA exhibits a weak and broad crystallization exotherm, with a crystallization temperature (*Tc*) close to 102°C (Fig. 5A), reflecting its intrinsically slow crystallization kinetics. Upon incorporation of mussel shell powder, *Tc* shifts slightly toward lower temperatures (around 98°C–100°C) but then remains nearly constant for all composite samples, regardless of filler loading (Table 2). This shift toward lower crystallization temperatures suggests that the mussel shell particles may act as heterogeneous nucleation sites, facilitating the onset of crystallization during cooling. This behavior indicates that the introduction of a relatively small amount of mineral filler is sufficient to promote heterogeneous nucleation phenomena in PLLA. Once an adequate density of nucleation sites is reached, further increases in filler content do not significantly alter the temperature at which crystallization occurs. In this regime, the crystallization process becomes governed primarily by polymer chain mobility and crystal growth rather than nucleation density.

The crystallization enthalpy, corrected to account for the PLLA mass fraction, shows a non-monotonic dependence on filler content. Δ*Hc* of PLLA increases strongly at low filler loadings and reaches a maximum at approximately 20 wt% mussel shell powder (Fig. 5A and Table 2). This behavior suggests the presence of an optimal filler concentration at which nucleation efficiency and polymer chain mobility are balanced, resulting in the highest crystallizable fraction. This enhancement is consistent with a nucleation-promoting effect of the mussel shell particles, which promote the formation of a higher crystalline fraction during cooling. At higher filler contents, Δ*Hc* decreases progressively, indicating that the beneficial nucleation effect is progressively counterbalanced by confinement and dilution effects [52]. At high mineral loadings, polymer chains experience restricted mobility near rigid filler surfaces and the effective volume available for crystal growth is reduced, limiting the extent of crystallization despite the presence of abundant nucleation sites [53].

The crystallization conversion curves (Fig. 5B) further support this interpretation. All PLLA/mussel shell powder composites exhibit very similar sigmoidal conversion profiles, suggesting comparable overall crystallization kinetics once heterogeneous nucleation is established. In contrast, neat PLLA shows a slightly earlier onset of conversion, consistent with homogeneous nucleation occurring at higher temperatures. The close overlap of the conversion curves suggests that increasing filler content beyond a certain threshold does not significantly accelerate crystallization, and that crystal growth rather than nucleation may become the rate-limiting step. These results are consistent with the presence of heterogeneous nucleation sites in PLLA composites, while not allowing a quantitative assessment of nucleation efficiency.

DSC heating scans performed after rapid quenching provide complementary insight into crystallization under conditions where the polymer initially lacks an ordered structure (Fig. 6A). All samples exhibit a glass

transition around 57°C–58°C, followed by cold crystallization and subsequent melting. The glass transition temperature remains essentially unchanged with filler content, indicating that the presence of mussel shell powder does not significantly alter the segmental dynamics at the glass transition. This observation suggests that the filler primarily influences crystallization behavior rather than the fundamental molecular mobility of PLLA chains in the amorphous phase.

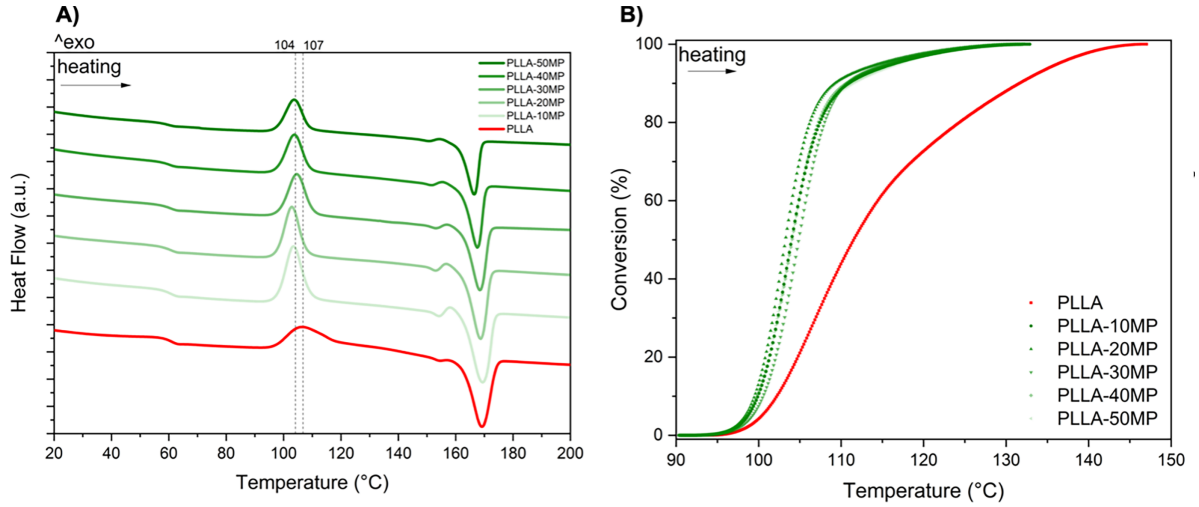

Figure 6: (**A**) Heating scans and (**B**) conversion rate of PLLA and PLLA/mussel shell powder composites (10%–50% *w/w*) recorded by DSC at 10°C/min after quenching.

However, the heat capacity step at T_g (ΔCp) decreases markedly for filler contents above 40 wt% (Table 3). This reduction in ΔCp reflects a decrease in the fraction of mobile amorphous PLLA chains, consistent with increased confinement and interfacial interactions at high filler loadings. The saturation of the polymer-filler interface at elevated mineral contents restricts chain mobility and reduces the thermodynamic contribution of the amorphous phase.

Cold crystallization during heating occurs at temperatures between 104°C and 107°C (Fig. 6A). Compared to neat PLLA, the presence of mussel shell powder induces a slight shift of *Tc* toward lower temperatures, from about 107°C for PLLA to approximately 103°C–104°C for the composites (Table 3). This shift is consistent with a heterogeneous nucleation contribution from the mussel shell particles, which facilitate crystallization upon heating from the amorphous state. The crystallization enthalpy, when normalized to the PLLA mass fraction, remains relatively stable across all composite formulations, indicating that the overall crystallizable fraction of PLLA is not strongly affected by filler content under heating conditions. Nevertheless, the intensity of the cold crystallization exotherm decreases progressively with increasing filler content, reflecting the dilution of the polymer phase.

The conversion curves derived from the heating scans (Fig. 6B) reveal clear differences between neat PLLA and the composites. Neat PLLA exhibits significantly slower crystallization kinetics, with conversion occurring over a broader temperature range. In contrast, all PLLA/mussel shell powder composites display much steeper and closely overlapping conversion curves, indicating faster and more uniform crystallization once nucleation is facilitated by the filler. This behavior further supports the hypothesis that mussel shell powder may reduce the crystallization barrier of PLLA, although no quantitative kinetic parameters can be extracted from the present analysis.

Comparing crystallization during cooling and cold crystallization upon heating reveals both similarities and important differences. In both cases, the addition of mussel shell powder suggests the activation of heterogeneous nucleation mechanisms [54], leading to similar crystallization temperatures for all composites and overlapping conversion curves. This indicates that, once nucleation is no longer limiting, crystallization kinetics are primarily controlled by PLLA chain mobility and growth processes. However, the influence of filler content on crystallization enthalpy differs between the two thermal histories. During cooling, ΔHc exhibits a clear maximum at intermediate filler content (~20 wt%), reflecting an optimal balance between nucleation efficiency and chain mobility. During heating after quenching, ΔHc of PLLA remains relatively constant, suggesting that cold crystallization is less sensitive to filler-induced confinement effects, as crystallization occurs from a highly disordered amorphous state with increased chain mobility above *Tg*.

Furthermore, no significant shift in thermal transitions was observed, suggesting that severe chain scission during processing is unlikely. This supports the interpretation that the changes in properties are mainly governed by filler–matrix interactions.

3.6 Thermomechanical Properties (DMA)

Dynamic mechanical analysis was performed to investigate the viscoelastic properties of PLLA/mussel shell powder composites and to assess the effect of filler loading on the glass transition and stiffness of the materials (Table 4).

Table 4: Glass transition temperature and viscoelastic properties of PLLA/mussel shell powder composites obtained by DMA. The table summarizes the tan δ peak temperature (*Tg*), full width at half maximum (FWHM) of the transition, peak of the loss modulus (E''), and storage modulus at 20°C.

PLLA/Mussel Shell Powder Ratio (*w/w*)	$T_{\tan\delta peak}$ (°C)	$FWHM_{\tan\delta peak}$ (°C)	$T_{E''peak}$ (°C)	$E'_{20°C}$ (MPa)
100/0	58.9	7.5	52.1	2434
90/10	58.7	7.9	51.6	2792
80/20	59.9	7.4	54.4	3094
70/30	59.3	7.3	52.9	2988
60/40	60.9	8.9	54.0	3455
50/50	60.8	9.0	54.5	4163

As shown in Fig. 7A, the storage modulus at 20°C ($E'_{20°C}$) increased steadily with mussel shell powder content, from 2434 MPa for neat PLLA to 4163 MPa at 50% *w/w*. This substantial increase in storage modulus demonstrates the strong reinforcing effect of the rigid mineral filler within the PLLA matrix. This improvement in stiffness highlights the mechanical reinforcing effect of the mussel shell powder, attributed to its intrinsic rigidity and its ability to restrict polymer chain motion through interfacial interactions [55]. The presence of inorganic particles limits the mobility of surrounding polymer chains, leading to a stiffer composite material even at relatively low filler contents.

The glass transition temperature (*Tg*) was evaluated using both the peak of the tan δ and the peak of the loss modulus (E''). For neat PLLA, T_g values were 58.9°C (tan δ peak) (Fig. 7B) and 52.1°C (E'' peak). With increasing mussel content, both indicators showed a slight but consistent increase: up to 60.8°C (tan δ) and 54.5°C (E'') for the 50% composite. This slight shift in T_g suggests a moderate restriction of segmental mobility in the amorphous phase due to the presence of rigid filler particles and interfacial interactions between the mineral surface and the polymer matrix. This indicates a moderate reduction

in segmental mobility due to the presence of the filler, though the nature of the glass transition remains relatively unaffected.

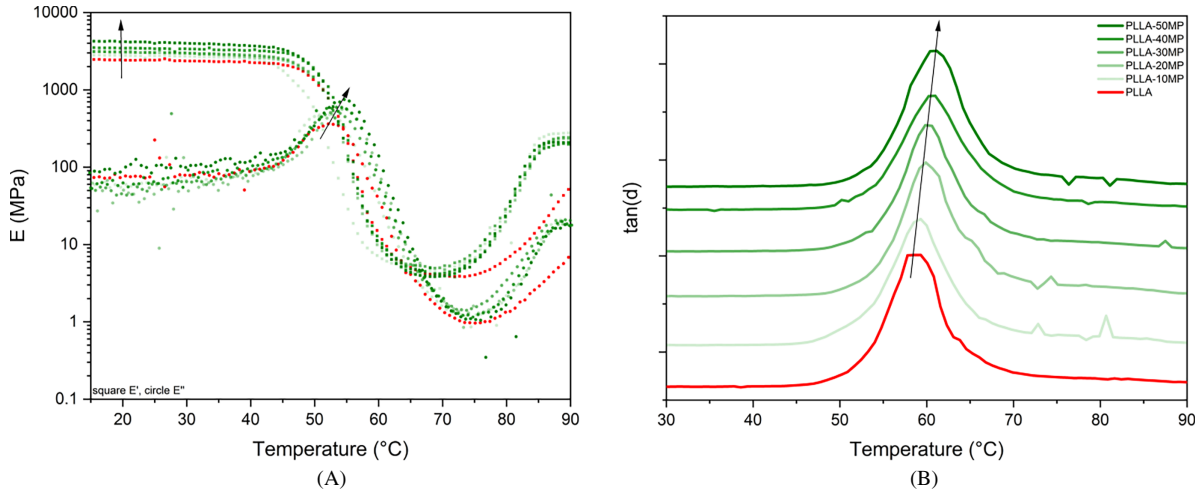

Figure 7: (**A**) Storage and loss modulus and (**B**) tan δ vs. temperature for PLLA/mussel shell powder composites (0%–50% *w/w*).

In addition to the shift in stiffness in the glassy region, a marked increase in storage modulus is observed upon heating above T_g for all samples (Fig. 7A). This modulus recovery corresponds to the occurrence of cold crystallization [56], during which newly formed crystalline domains act as physical crosslinks and reinforce the material in the rubbery state.

Notably, this post-T_g stiffening occurs at lower temperatures and with a steeper modulus increase for all PLLA/mussel shell powder composites compared to neat PLLA. This shift toward lower crystallization temperatures is consistent with the DSC results, which demonstrated that mussel shell powder acts as a heterogeneous nucleating agent for PLLA. This behavior indicates that the presence of mussel shell powder accelerates crystallization upon heating, independently of the exact filler content. This observation is fully consistent with the DSC heating results, which show a shift of the cold crystallization temperature toward lower values for all composites and faster crystallization kinetics compared to neat PLLA.

The close similarity of the modulus recovery profiles among the composites further suggests that, once heterogeneous nucleation is activated by the filler, crystallization kinetics are governed primarily by PLLA chain mobility rather than by the filler concentration. Therefore, the DMA results confirm that mussel shell powder not only reinforces the polymer matrix but also modifies the crystallization behavior of PLLA, contributing to improved thermomechanical performance of the composites.

The full width at half maximum (FWHM) of the tan δpeak increased from 7.5°C to 9.0°C across the composition range, suggesting a progressive broadening of the glass transition. This broadening reflects increased microstructural heterogeneity in the composite system, likely arising from interfacial regions between the PLLA matrix and the dispersed mineral particles. This behavior is consistent with increased microstructural heterogeneity caused by the presence of rigid filler particles and possible interfacial zones with constrained chain mobility.

Taken together, these results demonstrate that mussel shell powder significantly increases the stiffness of PLLA while only moderately altering its thermal relaxation behavior. The combination of enhanced crystallization and mechanical reinforcement highlights the potential of biogenic calcium carbonate from mussel shells as an effective functional filler for tailoring the thermomechanical properties of PLLA-based

materials. The composite remains predominantly governed by the PLLA matrix but with increasingly pronounced interfacial interactions as filler content rises.

3.7 Mechanical Performance (Tensile Testing)

Tensile tests were conducted on PLLA/mussel shell powder composites containing 0 to 50 wt% filler to evaluate the influence of mussel powder incorporation on mechanical performance in the solid state. The main parameters analyzed were Young's modulus (E), tensile strength (σ_{max}), strain at break (ε), stress at rupture (σ_{rup}), and toughness (area under the stress-strain curve) and summarized in Fig. 8.

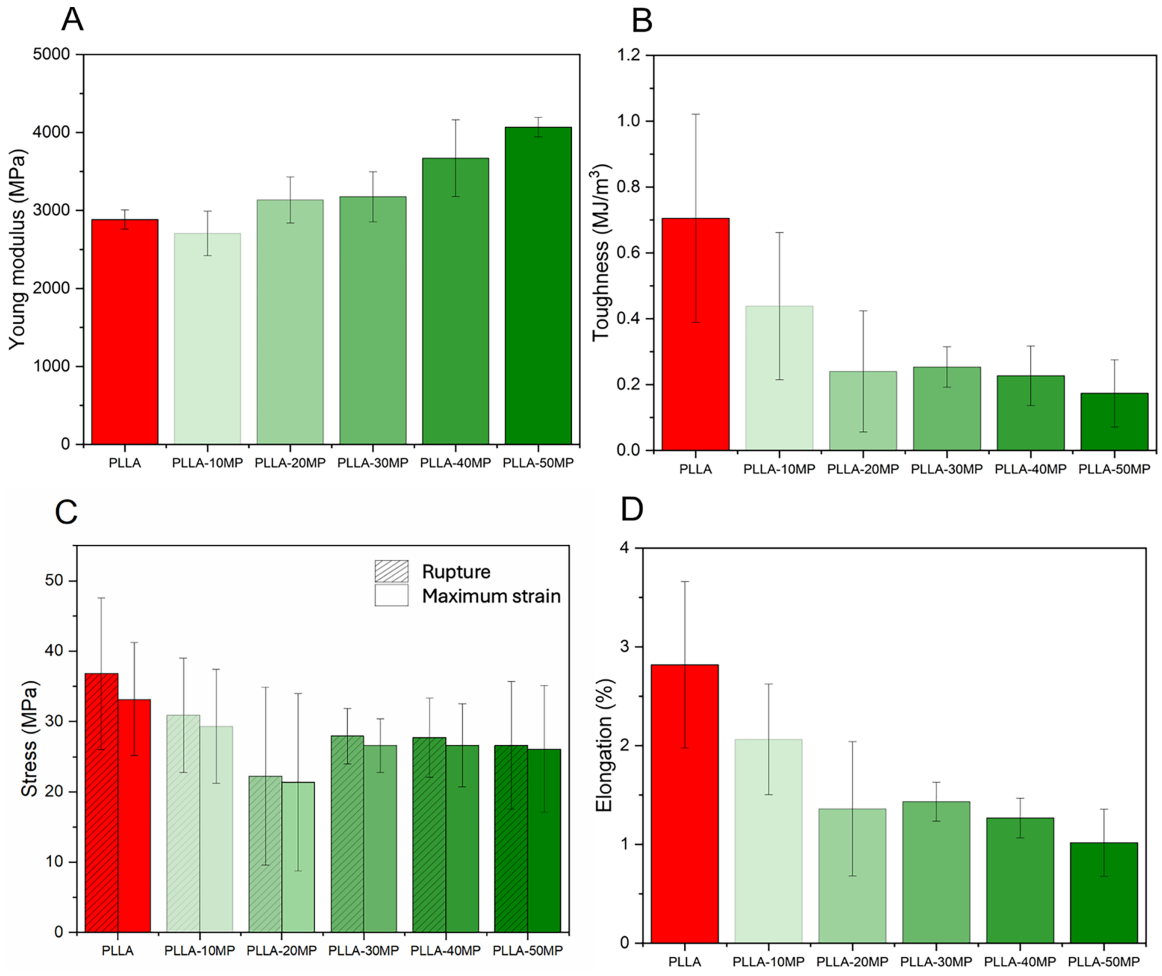

Figure 8: Tensile properties of PLLA/mussel shell powder composites (0%–50% *w/w*). Mechanical performance as a function of mussel powder content showing (**A**) Young's modulus (E), (**B**) toughness, (**C**) maximum stress (σ_{max}), stress at rupture (σ_{rup}), and (**D**) elongation at break.

The Young's modulus increased overall with increasing mussel content, from 2883 ± 123 MPa for neat PLLA to a maximum of 4068 ± 126 MPa at 50 wt% filler, showing a clear stiffening effect. This increase in modulus reflects the reinforcing contribution of the rigid mineral particles, which act as load-bearing elements within the polymer matrix. This trend aligns with DMA results and is attributed to the rigid, mineral nature of the mussel shell powder, which reinforces the polymer matrix and resists deformation under tensile loading. In addition, the presence of dispersed inorganic particles restricts polymer chain mobility and

contributes to an overall increase in composite stiffness. A moderate deviation from this trend was observed at 10%, likely due to local heterogeneities or variability in dispersion.

In contrast, both tensile strength (σ_{max}) and elongation at break (ε) decreased upon filler addition. The maximum strength dropped from 36.8 ± 10.8 MPa (0%) to 26.6 ± 9.1 MPa (50%), while elongation at break decreased from 2.8% ± 0.8% to 1.0% ± 0.3%. Such reductions in tensile strength and ductility are commonly observed in mineral-filled thermoplastic composites and reflect the typical stiffness-toughness trade-off associated with rigid particle reinforcement. The decrease in elongation at break indicates that the incorporation of mineral particles reduces the ability of the polymer matrix to undergo plastic deformation.

Representative stress-strain curves of neat PLLA and PLLA/mussel shell powder composites are shown in Fig. 9. Neat PLLA exhibits a progressive increase in stress with strain up to failure, with slight deviation from linearity prior to rupture, indicating the onset of localized plastic deformation and incipient necking. In contrast, the addition of mussel shell powder leads to a marked reduction in elongation at break and a more abrupt failure, particularly at high filler contents, reflecting a transition toward a more brittle mechanical behavior. The reduction in ductility is attributed to the presence of rigid mineral particles, which restrict chain mobility and act as stress concentration sites. Under tensile loading, PLLA deformation involves chain orientation and partial structural disordering within the amorphous phase; however, the incorporation of filler limits this molecular rearrangement, thereby suppressing neck propagation and promoting earlier failure.

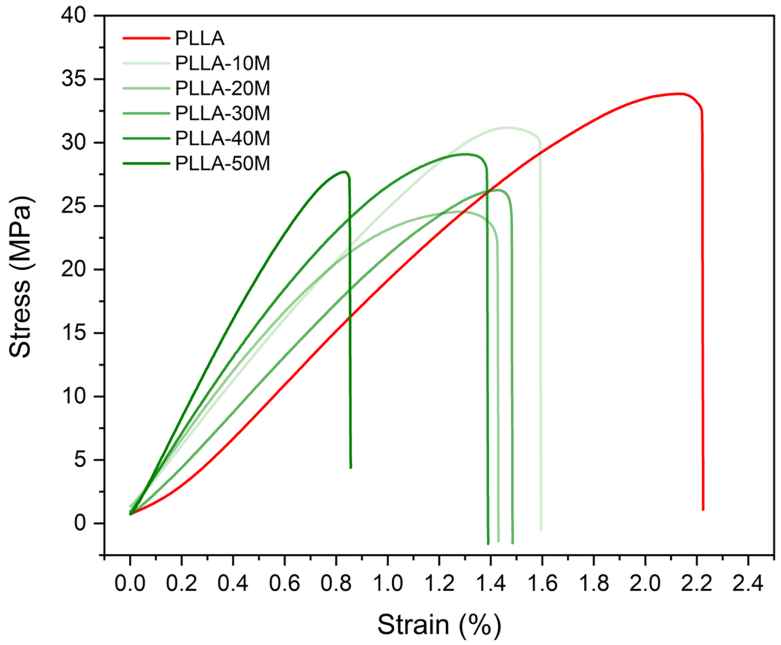

Figure 9: Representative stress-strain curves of neat PLLA and PLLA/mussel shell powder composites (10–50 wt%) under tensile loading.

This behavior may be attributed to stress concentration effects at the polymer-filler interface and the limited deformability of the rigid calcium carbonate particles. Under tensile loading, these heterogeneities can initiate microcracks or localized stress concentrations, which reduce the overall ductility of the material. Nevertheless, the composites retain a relatively stable mechanical response across the investigated filler contents.

The overall toughness of the composites also decreased with increasing filler loading, following the reduction in elongation at break. This reduction in toughness is consistent with the restricted chain mobility and increased stiffness observed in the DMA analysis. The presence of rigid particles limits the capacity of the polymer matrix to dissipate mechanical energy during deformation.

Despite the reduction in ductility and toughness, the substantial increase in Young's modulus demonstrates the effectiveness of mussel shell powder as a reinforcing filler for PLLA. These results highlight the potential of biogenic calcium carbonate derived from mussel shells to enhance stiffness while maintaining acceptable mechanical performance for applications where rigidity is required.

Although PLLA may undergo some degree of thermal degradation at elevated processing temperatures, the observed mechanical trends are consistent with typical mineral-filled thermoplastics. The increase in stiffness and the reduction in tensile strength and elongation at break are therefore primarily attributed to filler-induced effects such as stress concentration and reduced chain mobility, rather than dominant molecular weight degradation.

4 Conclusion

This study demonstrated the successful incorporation of mussel shell waste as a bio-derived mineral filler in PLLA-based composites. The mussel shells, composed primarily of biogenic calcium carbonate, were processed into powder and incorporated into PLLA at filler loadings ranging from 10 to 50 wt%. Comprehensive characterization was performed to evaluate the influence of the filler on the morphological, thermal, crystallization, thermomechanical, and mechanical properties of the resulting composites.

The results showed that mussel shell powder suggests a heterogeneous nucleation effect in PLLA, significantly enhancing crystallization during both cooling and heating conditions. Differential scanning calorimetry revealed that the presence of the biogenic calcium carbonate particles promotes crystallization and modifies crystallization kinetics, with an optimal crystallization behavior observed at intermediate filler contents. These findings highlight the ability of mussel shell powder to tailor the semicrystalline structure of PLLA. More specifically, an increase in crystallization enthalpy and a shift in crystallization temperature were observed, confirming the influence of the filler on the crystallization behavior of PLLA.

Dynamic mechanical analysis further demonstrated a substantial increase in thermomechanical stiffness with increasing filler content. The storage modulus increased markedly across the composite series, confirming the strong reinforcing effect of the rigid mineral filler. At the same time, only minor changes in the glass transition temperature were observed, indicating that the filler primarily influences crystallization and mechanical reinforcement rather than fundamentally altering the segmental dynamics of the polymer matrix. At the highest filler content, the storage modulus increased by more than 70%, highlighting the significant stiffening effect of the biogenic filler.

Tensile testing confirmed the reinforcing effect of the mussel shell particles, with a significant increase in Young's modulus as filler content increased. As expected for mineral-filled thermoplastic composites, a progressive reduction in tensile strength, elongation at break, and toughness was observed, reflecting the typical stiffness–ductility trade-off associated with rigid particle reinforcement. This mechanical behavior is consistent with increased stress concentration and restricted polymer chain mobility at higher filler loadings.

Overall, this work demonstrates that mussel shell waste can serve as an effective biogenic calcium carbonate filler capable of enhancing the crystallization behavior and thermomechanical stiffness of PLLA. Beyond providing mechanical reinforcement, the mussel shell particles appear to promote nucleation phenomena, contributing to modifications of the semicrystalline structure of the polymer. These results highlight a promising pathway for the valorization of marine bio-waste while contributing to the development of

sustainable polymer composites with improved structural performance. Such materials show potential for applications in packaging, disposable items, and semi-structural components where increased stiffness, reduced material cost, and improved environmental footprint are required.

Acknowledgement: Not applicable.

Funding Statement: The authors received no specific funding for this study.

Author Contributions: The authors confirm contribution to the paper as follows: study conception and design: Nathan Jourdainne: Conceptualization, Methodology, Validation, Formal analysis, Investigation, Writing—original draft, Visualization. Mathilda Ekholm: Conceptualization, Investigation. Nawel Belkessa: Investigation. Antonin Vignon: Investigation. Nicolas Sbirrazzuoli: Resources, Supervision, Project administration. Christelle Combeaud: Resources, Project administration. Jean-Luc Bouvard: Resources, Project administration. Nathanael Guigo: Conceptualization, Validation, Resources, Writing—review & editing, Supervision, Project administration, Funding acquisition. All authors reviewed and approved the final version of the manuscript.

Availability of Data and Materials: The data that support the findings of this study are available from the corresponding author upon reasonable request.

Ethics Approval: Not applicable.

Conflicts of Interest: The authors declare no conflicts of interest.

References

1. OECD. Improving resource efficiency and the circularity of economies for a greener world. Paris, France: OECD; 2020. 25 p. doi:10.1787/1b38a38f-en.
2. Thormann L, Neuling U, Kaltschmitt M. Opportunities and challenges of the European green deal for the chemical industry: an approach measuring circularity. Clean Circ Bioecon. 2023;5:100044. doi:10.1016/j.clcb.2023.100044.
3. Trubiano F. From carbon to human health: lifecycle of fossil fuels, toxic polymers and social justice in Philadelphia. In: Proceedings of the 2020 AIA/ACSA Intersections Research Conference: CARBON; 2020 Sep 30–Oct 2; Online. Washington, DC, USA: ACSA Press; 2020. p. 184–90. doi:10.35483/ACSA.AIA.FallInterCarbon.20.28.
4. Wang Z, Ganewatta MS, Tang C. Sustainable polymers from biomass: bridging chemistry with materials and processing. Prog Polym Sci. 2020;101:101197. doi:10.1016/j.progpolymsci.2019.101197.
5. Olivetti EA, Cullen JM. Toward a sustainable materials system. Science. 2018;360(6396):1396–8. doi:10.1126/science.aat6821.
6. Nofar M, Sacligil D, Carreau PJ, Kamal MR, Heuzey MC. Poly (lactic acid) blends: processing, properties and applications. Int J Biol Macromol. 2019;125(25):307–60. doi:10.1016/j.ijbiomac.2018.12.002.
7. Kawashima N, Yagi T, Kojima K. Pilot-scale composting test of polylactic acid for social implementation. Sustainability. 2021;13(4):1654. doi:10.3390/su13041654.
8. da Silva D, Kaduri M, Poley M, Adir O, Krinsky N, Shainsky-Roitman J, et al. Biocompatibility, biodegradation and excretion of polylactic acid (PLA) in medical implants and theranostic systems. Chem Eng J. 2018;340:9–14. doi:10.1016/j.cej.2018.01.010.
9. Ramezani Dana H, Ebrahimi F. Synthesis, properties, and applications of polylactic acid-based polymers. Polym Eng Sci. 2023;63(1):22–43. doi:10.1002/pen.26193.
10. Taib NAB, Rahman MR, Huda D, Kuok KK, Hamdan S, Bin Bakri MK, et al. A review on poly lactic acid (PLA) as a biodegradable polymer. Polym Bull. 2023;80(2):1179–213. doi:10.1007/s00289-022-04160-y.
11. Jałbrzykowski M, Oksiuta Z, Obidziński S, Czyżewska U, Osiecki T, Kroll L, et al. Assessment of innovative PLA biopolymer compositions with plant waste fillers. Eng Fail Anal. 2022;139(8–9):106496. doi:10.1016/j.engfailanal.2022.106496.

12. Wan Z, Li M, Zhuang Y, Tong Z. Effect of electrospun stereo complex PLA fibers and modified cellulose nanocrystals on crystallization of poly(L-lactic acid). J Appl Polym Sci. 2023;140(19):e53839. doi:10.1002/app.53839.
13. Dobrzyńska-Mizera M, Knitter M, Woźniak-Braszak A, Baranowski M, Sterzyński T, Di Lorenzo ML. Poly(l-lactic acid)/pine wood bio-based composites. Materials. 2020;13(17):3776. doi:10.3390/ma13173776.
14. Yadav R, Singh M, Shekhawat D, Lee SY, Park SJ. The role of fillers to enhance the mechanical, thermal, and wear characteristics of polymer composite materials: a review. Compos Part A Appl Sci Manuf. 2023;175(4):107775. doi:10.1016/j.compositesa.2023.107775.
15. Post W, Kuijpers LJ, Zijlstra M, van der Zee M, Molenveld K. Effect of mineral fillers on the mechanical properties of commercially available biodegradable polymers. Polymers. 2021;13(3):394. doi:10.3390/polym13030394.
16. Injorhor P, Trongsatitkul T, Wittayakun J, Ruksakulpiwat C, Ruksakulpiwat Y. Nano-hydroxyapatite from White Seabass scales as a bio-filler in polylactic acid biocomposite: preparation and characterization. Polymers. 2022;14(19):4158. doi:10.3390/polym14194158.
17. Haylock R, Rosentrater KA. Cradle-to-grave life cycle assessment and techno-economic analysis of polylactic acid composites with traditional and bio-based fillers. J Polym Environ. 2018;26(4):1484–503. doi:10.1007/s10924-017-1041-2.
18. Lendvai L, Omastova M, Patnaik A, Dogossy G, Singh T. Valorization of waste wood flour and rice husk in poly(lactic acid)-based hybrid biocomposites. J Polym Environ. 2023;31(2):541–51. doi:10.1007/s10924-022-02633-9.
19. Tichy M, Valášek P, Müller M. Wear resistance of bio-polymer composite base on cotton post-harvest line residues. Mater Sci Forum. 2023;1090(4):3–8. doi:10.4028/p-z02z0z.
20. Jakab SK, Singh T, Fekete I, Lendvai L. Agricultural by-product filled poly(lactic acid) biocomposites with enhanced biodegradability: the effect of flax seed meal and rapeseed straw. Compos Part C Open Access. 2024;14(10):100464. doi:10.1016/j.jcomc.2024.100464.
21. Sogut E, Cakmak H. Utilization of carrot (*Daucus carota* L.) fiber as a filler for chitosan based films. Food Hydrocoll. 2020;106(5):105861. doi:10.1016/j.foodhyd.2020.105861.
22. Da D. Structural design against brittle fracture: optimizing energy release rate and experiment. Comput Meth Appl Mech Eng. 2024;425(6):116935. doi:10.1016/j.cma.2024.116935.
23. Li Z, Chen F. A toughness-based crack initiation-propagation criterion using a modified fracture energy parameter. Eng Fract Mech. 2022;269(5):108536. doi:10.1016/j.engfracmech.2022.108536.
24. Lapčík L, Maňas D, Lapčíková B, Vašina M, Staněk M, Čépe K, et al. Effect of filler particle shape on plastic-elastic mechanical behavior of high density poly(ethylene)/mica and poly(ethylene)/wollastonite composites. Compos Part B Eng. 2018;141(1–2):92–9. doi:10.1016/j.compositesb.2017.12.035.
25. Letwaba J, Muniyasamy S, Rakku N, Mavhungu L. Improved performance and compost biodegradation of PLA/PBAT blend and PLA/PBAT compatibilized blends with algae as a reinforcer. J Renew Mater. 2026;14(2):1–10. doi:10.32604/jrm.2025.02025-0132.
26. Ramesh P, Vinodh S. State of art review on Life Cycle Assessment of polymers. Int J Sustain Eng. 2020;13(6):411–22. doi:10.1080/19397038.2020.1802623.
27. Cooney R, de Sousa DB, Fernández-Ríos A, Mellett S, Rowan N, Morse AP, et al. A circular economy framework for seafood waste valorisation to meet challenges and opportunities for intensive production and sustainability. J Clean Prod. 2023;392(24):136283. doi:10.1016/j.jclepro.2023.136283.
28. Tamasiga P, Miri T, Onyeaka H, Hart A. Food waste and circular economy: challenges and opportunities. Sustainability. 2022;14(16):9896. doi:10.3390/su14169896.
29. Piras S, Salathia S, Guzzini A, Zovi A, Jackson S, Smirnov A, et al. Biomimetic use of food-waste sources of calcium carbonate and phosphate for sustainable materials—a review. Materials. 2024;17(4):843. doi:10.3390/ma17040843.
30. Chakraborty A, Parveen S, Chanda DK, Aditya G. An insight into the structure, composition and hardness of a biological material: the shell of freshwater mussels. RSC Adv. 2020;10(49):29543–54. doi:10.1039/d0ra04271d.
31. Xu J, Mucalo MR, Pickering KL. Bioinspired surface modification of mussel shells and their application as a biogenic filler in polypropylene composites. Compos Part C Open Access. 2024;15(2):100520. doi:10.1016/j.jcomc.2024.100520.

32. Cangiotti J, Scatto M, Araya-Hermosilla E, Micheletti C, Crivellari D, Balloni A, et al. Valorization of seashell waste in polypropylene composites: an accessible solution to overcome marine landfilling. Eur Polym J. 2022;162:110877. doi:10.1016/j.eurpolymj.2021.110877.
33. Hou X, Liu Y, Zheng T, Zheng Z, Sun J, Xiong M, et al. Multi-scale design of the structure and mechanical performance of the deep-sea hydrothermal mussel (*Bathymodiolus aduloides*) shell. J Mech Behav Biomed Mater. 2025;172:107188. doi:10.1016/j.jmbbm.2025.107188.
34. Chen K, Wang Y, Tuo Z, Cui J, Zhang Y, Lin Z, et al. Design and study of biomimetic resin matrix composites based on shellfish structure. J Reinf Plast Compos. 2025;44(15–16):939–50. doi:10.1177/07316844241233437.
35. Liang JZ, Zhou L, Tang CY, Tsui CP. Crystalline properties of poly(L-lactic acid) composites filled with nanometer calcium carbonate. Compos Part B Eng. 2013;45(1):1646–50. doi:10.1016/j.compositesb.2012.09.086.
36. Ding Y, Xin Y. Molecular dynamics simulation of calcium carbonate nano filled PLA/PPC composites: interfacial properties and water vapor barrier. Discov Nano. 2025;20(1):85. doi:10.1186/s11671-025-04223-9.
37. Patanair B, Saiter-Fourcin A, Thomas S, Thomas MG, Parathukkamparambil Pundarikashan P, Gopalan Nair K, et al. Promoting interfacial interactions with the addition of lignin in poly(lactic acid) hybrid nanocomposites. Polymers. 2021;13(2):272. doi:10.3390/polym13020272.
38. Gigante V, Cinelli P, Righetti MC, Sandroni M, Tognotti L, Seggiani M, et al. Evaluation of mussel shells powder as reinforcement for PLA-based biocomposites. Int J Mol Sci. 2020;21(15):5364. doi:10.3390/ijms21155364.
39. Fu SY, Feng XQ, Lauke B, Mai YW. Effects of particle size, particle/matrix interface adhesion and particle loading on mechanical properties of particulate–polymer composites. Compos Part B Eng. 2008;39(6):933–61. doi:10.1016/j.compositesb.2008.01.002.
40. Rani GE, Murugeswari R, Siengchin S, Rajini N, Kumar MA. Quantitative assessment of particle dispersion in polymeric composites and its effect on mechanical properties. J Mater Res Technol. 2022;19(12):1836–45. doi:10.1016/j.jmrt.2022.05.147.
41. Kızılkaya B, Yıldız H, Acarlı S, Vural P. Investigation of the chemical composition of the shell structure of *Mytilus galloprovincialis* mussel from Kefken, Türkiye. Acta Nat Sci. 2024;5(1):57–68. doi:10.61326/actanatsci.v5i1.7.
42. Checa AG, Jiménez-López C, Rodríguez-Navarro A, Machado JP. Precipitation of aragonite by calcitic bivalves in Mg-enriched marine waters. Mar Biol. 2007;150(5):819–27. doi:10.1007/s00227-006-0411-4.
43. Kawano J, Maeda S, Nagai T. The effect of Mg^{2+} incorporation on the structure of calcium carbonate clusters: investigation by the anharmonic downward distortion following method. Phys Chem Chem Phys. 2016;18(4):2690–8. doi:10.1039/c5cp05139h.
44. Wang Q, Jiang F, Ouyang XK, Yang LY, Wang Y. Adsorption of Pb(II) from aqueous solution by mussel shell-based adsorbent: preparation, characterization, and adsorption performance. Materials. 2021;14(4):741. doi:10.3390/ma14040741.
45. Díaz E, Valle MB, Ribeiro S, Lanceros-Mendez S, Barandiarán JM. A new approach for the fabrication of cytocompatible PLLA-magnetite nanoparticle composite scaffolds. Int J Mol Sci. 2019;20(19):4664. doi:10.3390/ijms20194664.
46. Rocca-Smith JR, Lagorce-Tachon A, Iaconelli C, Bellat JP, Marcuzzo E, Sensidoni A, et al. How high pressure CO_2 impacts PLA film properties. Express Polym Lett. 2017;11(4):320–33. doi:10.3144/expresspolymlett.2017.31.
47. Fang Y, Zhao J, Zhang C, Li Y. Exothermic performance of the calcined limestone determined by exothermic temperature under fluidization during $CaCO_3$/CaO energy storage cycles. J Therm Sci. 2023;32(5):1784–96. doi:10.1007/s11630-023-1865-0.
48. Abdul Khalil HPS, Chong EWN, Owolabi FAT, Asniza M, Tye YY, Rizal S, et al. Enhancement of basic properties of polysaccharide-based composites with organic and inorganic fillers: a review. J Appl Polym Sci. 2019;136(12):47251. doi:10.1002/app.47251.
49. Charde SJ, Sonawane SS, Sonawane SH, Navin S. Influence of functionalized calcium carbonate nanofillers on the properties of melt-extruded polycarbonate composites. Chem Eng Commun. 2018;205(4):492–505. doi:10.1080/00986445.2017.1404459.

50. Shaiju P, Dorian BB, Senthamaraikannan R, Padamati RB. Biodegradation of poly (butylene succinate) (PBS)/stearate modified magnesium-aluminium layered double hydroxide composites under marine conditions prepared via melt compounding. Molecules. 2020;25(23):5766. doi:10.3390/molecules25235766.
51. Tian XK, Lin SC, Yan J, Zhao CY. Sintering mechanism of calcium oxide/calcium carbonate during thermochemical heat storage process. Chem Eng J. 2022;428(1):131229. doi:10.1016/j.cej.2021.131229.
52. Wang M, Li J, Shi G, Liu G, Müller AJ, Wang D. Suppression of the self-nucleation effect of semicrystalline polymers by confinement. Macromolecules. 2021;54(8):3810–21. doi:10.1021/acs.macromol.1c00485.
53. Piorkowska E. Crystallization in polymer composites and nanocomposites. In: Piorkowska E, Rutledge GC, editors. Handbook of polymer crystallization. Hoboken, NJ, USA: John Wiley & Sons, Inc.; 2013. p. 379–98. doi:10.1002/9781118541838.ch13.
54. Wadkin-Snaith D, Mulheran P, Johnston K. Filler-induced heterogeneous nucleation of polymer crystals investigated by molecular dynamics simulations. Polymer. 2023;281(20):126113. doi:10.1016/j.polymer.2023.126113.
55. Ashok Kumar B, Saminathan R, Tharwan M, Vigneshwaran M, Sekhar Babu P, Ram S, et al. Study on the mechanical properties of a hybrid polymer composite using egg shell powder based bio-filler. Mater Today Proc. 2022;69(10):679–83. doi:10.1016/j.matpr.2022.07.114.
56. Fuller KNG, Gough J, Thomas AG. The effect of low-temperature crystallization on the mechanical behavior of rubber. J Polym Sci B Polym Phys. 2004;42(11):2181–90. doi:10.1002/polb.20091.